PHYSICAL REVIEW A **88**, 041403(R) (2013)

Electron shakeoff following the β^+ decay of trapped $^{35}Ar^+$ ions

C. Couratin,[1] X. Fabian,[1] B. Fabre,[2] B. Pons,[2] X. Fléchard,[1,*] E. Liénard,[1] G. Ban,[1] M. Breitenfeldt,[3] P. Delahaye,[4] D. Durand,[1] A. Méry,[5] O. Naviliat-Cuncic,[1,6] T. Porobic,[3] G. Quéméner,[1] D. Rodríguez,[7] N. Severijns,[3] J.-C. Thomas,[4] and S. Van Gorp[8]

[1]*LPC Caen, ENSICAEN, Université de Caen, CNRS/IN2P3, F-14070 Caen, France*

[2]*CELIA, Université Bordeaux, CNRS UMR 5107, CEA, 351 Cours de la Libération, F-33405 Talence, France*

[3]*Instituut voor Kern- en Stralingsfysica, Katholieke Universiteit Leuven, B-3001 Leuven, Belgium*

[4]*GANIL, CEA/DSM-CNRS/IN2P3, F-14070 Caen, France*

[5]*CIMAP, CEA/CNRS/ENSICAEN, BP 5133, F-14070 Caen, France*

[6]*NSCL and Department of Physics and Astronomy, Michigan State University, East Lansing, Michigan 48824, USA*

[7]*Departamento de Física Atómica, Molecular y Nuclear, Universitad de Granada, E-1871 Granada, Spain*

[8]*Atomic Physics laboratory, RIKEN, Saitama 351-0198, Japan*

(Received 27 June 2013; revised manuscript received 23 September 2013; published 16 October 2013)

The electron shakeoff of ^{35}Cl atoms resulting from the β^+ decay of $^{35}Ar^+$ ions has been investigated using a Paul trap coupled to a recoil-ion spectrometer. The charge-state distribution of the recoiling daughter nuclei is compared to theoretical calculations accounting for shakeoff and Auger processes. The calculations are in excellent agreement with the experimental results and enable one to identify the ionization reaction routes leading to the formation of all charge states.

DOI: 10.1103/PhysRevA.88.041403 PACS number(s): 32.80.Aa, 32.80.Hd, 79.20.Fv

Precise measurements of the recoil-ion energy spectra in nuclear β decay constitute sensitive tools to establish the vector axial vector structure of the weak interaction [1–3]. In particular, these measurements give access to the so-called β-ν angular correlation coefficient $a_{\beta\nu}$, which is sensitive to scalar and tensor exotic couplings excluded by the Standard Model of elementary particles [4]. The search for such exotic interactions has motivated new experiments using modern trapping techniques coupled to intense radioactive beams with high production rates [4]. Most of the ongoing experiments detect the β particles and the recoil ions in coincidence, providing a precise recoil-ion energy measurement using time-of-flight (TOF) techniques, and a precise control of systematic effects [5–7]. The LPCTrap setup [8,9], installed at GANIL, is based on the use of a Paul trap, to confine radioactive ions, coupled to a recoil-ion spectrometer. It has been recently upgraded to perform simultaneous measurements of both the charge state and the energy of the recoil ions. Fundamental atomic processes such as electron shakeoff (SO) resulting from the sudden change in the central potential can thus also be addressed through a measurement of the charge-state distribution of the recoiling ions. The setup has already enabled the measurement of electron SO in the decay of $^6He^+$ [10]. For this ideal textbook case, with only one electron, simple quantum calculations based on the sudden approximation (SA) could be tested with a relative precision of better than 4×10^{-4}. Beyond the prototypical $^6He^+$ case, heavier systems such as $^{35}Ar^+$ can reveal the role of more subtle shakeoff dynamics involving several electrons, and of subsequent relaxation processes such as the emission of Auger electrons. These multielectron processes, of paramount importance in atomic and molecular physics, have been mainly studied as postcollision mechanisms following the absorption of a photon in the x-ray spectral range (see, for instance, Refs. [11–14]). Alternatively, SO and Auger processes can be conveniently decoupled within multielectron rearrangements induced by sudden nuclear β decay. These ionization mechanisms have been explored for a large variety of β^- emitters [15]. In contrast, information is scarce for β^+ decaying parent atoms [6,16,17] and even totally missing, to our knowledge, for multielectronic singly charged systems. Thus here we investigate the charge-state distribution following β^+ emission of $^{35}Ar^+$. In addition to be interesting *per se*, it is worth noting that SO further can be a source of systematic error for β-ν angular correlation coefficient measurements. This systematic error, which was found to be small in a previous LPCTrap experiment on $^6He^+$ decay [7], would become problematic for many electron systems. For the weak interaction trap for charged particles (WITCH) setup [18] installed at ISOLDE-CERN, whose main goal is to measure $a_{\beta\nu}$ in the decay of $^{35}Ar^+$ ions confined in a Penning trap, an independent measurement of the charge-state distribution of the recoil ions will ease the analysis and improve the precision [19].

The experimental setup has been previously described in detail [8–10]. The radioactive ^{35}Ar nuclei were produced at the SPIRAL target-electron cyclotron resonance (ECR) ion source system of GANIL, Caen, France, by a primary beam of ^{36}Ar ions impinging on a graphite target. After mass separation the $^{35}Ar^+$ ions were guided at 10 keV through the LIRAT low-energy beam line. At the entrance of the LPCTrap apparatus, the $^{35}Ar^+$ beam intensity was typically 10^7 pps. The ions were first injected in a radio-frequency cooler and buncher (RFQCB) [20] for beam preparation. This linear Paul trap, mounted on a high-voltage platform to decelerate the ions down to 50 eV, was filled with He buffer gas at a pressure of 1.6×10^{-2} mbar to cool down the ions below 1 eV. The $^{35}Ar^+$ ions from LIRAT were continuously injected in the RFQCB, cooled, and accumulated into bunches before being extracted with a cycle period of 200 ms. They were then reaccelerated downstream using a pulsed cavity, transported between the two traps with a kinetic energy of about 1 keV, and decelerated down to 100 eV by a second pulsed cavity located at the entrance of the measurement transparent Paul trap (MTPT).

*fleched@lpccaen.in2p3.fr

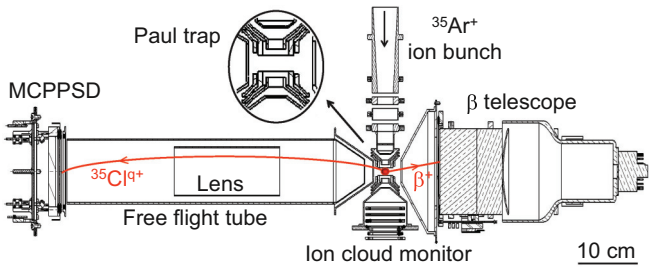

FIG. 1. (Color online) Top view of the experimental setup. The inset shows the structure of the six stainless-steel rings of the Paul trap. See text for details.

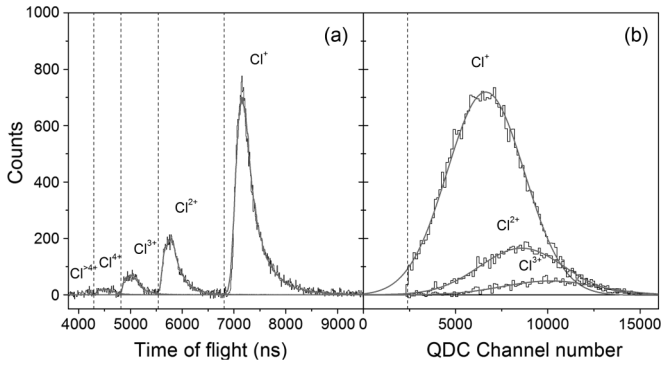

FIG. 2. (a) Experimental (black line) and simulated TOF spectra associated with the different charge states (gray lines); vertical dashed lines indicate the ranges of integration used to obtain the charge-state branching ratios. (b) Charge collected from the MCPPSD for different recoil-ion charge states (black lines) adjusted with gaussians (gray lines); the vertical dashed line indicates the cut due to electronic threshold.

For each injection cycle, an average of about 2×10^3 $^{35}Ar^{+}$ ions were successfully trapped and confined by applying a 0.48 MHz rf voltage of 120 V_{pp} to the two inner rings of the MTPT (Fig. 1). Helium buffer gas at a pressure of 10^{-5} mbar was also used in the MTPT chamber to further cool down the trapped ions. The β particles and the recoiling ions resulting from the β decay of the trapped $^{35}Ar^{+}$ ions were detected in coincidence using detectors located around the trap (Fig. 1). The β telescope, composed of a thin double-sided silicon strip detector followed by a plastic scintillator, provides the position and the energy of the incoming β particles. The signal from the plastic scintillator also defines the reference time for a decay event. A recoil-ion spectrometer enables one to separate the charge states of the recoiling ions using their time of flight (TOF). Ions emitted towards the recoil-ion spectrometer first cross a collimator through a 90% transmission grid (set at ground potential). They are then accelerated by a -2 kV potential applied to a free flight tube (Fig. 1) whose entrance and exit are defined by two additional 90% transmission grids. Inside the tube, an electrostatic lens at -250 V permits a 100% collection efficiency of the ions by a microchannel plate position-sensitive detector (MCPPSD) [21]. A -4 kV voltage applied on the front plate of the MCPPSD ensures a detection efficiency close to maximum for all charge states of the recoil ions, independently of their initial kinetic energy.

For each detected event, the energy and position of the β particle, the time of flight (TOF) and position of the recoil ion, were recorded. The procedure applied for the detector calibrations was identical to that described in Ref. [7]. Only events corresponding to a β particle depositing more than 0.4 MeV in the scintillator were kept in the analysis. The TOF distribution measured for the $^{35}Cl^{q+}$ recoil ions resulting from $^{35}Ar^{+}$ β decay is shown in Fig. 2(a). A constant background in TOF due to uncorrelated signals from the recoil ion and β detectors has been subtracted from the data.

The experimental charge-state branching ratios and their associated statistical uncertainties were simply deduced from the integration of counts within the TOF selection windows displayed on Fig. 2(a). Two additional corrections, labeled $\text{Tail}_{\text{corr.}}$ and $\text{MCP}_{\text{corr.}}$ in Table I, were then applied. The first takes into account the tails of charge distributions extending beyond their respective integration windows. TOF spectra associated with each charge state were generated using Monte Carlo simulations [7,10] and were adjusted to the experimental data. Several ingredients of the simulations, such as the exact size of the trapped ion cloud, weak decay branches of ^{35}Ar towards excited states, and possible scattering of the β particles on parts of the trapping chamber, were neglected or approximated. Therefore, a conservative relative uncertainty of 10% was applied on these corrections. The second correction concerns the dependence of the MCPPSD detection efficiency on the charge state of the recoil ions. The loss of detected events due to electronic threshold was precisely estimated by fitting the charge distributions collected from the recoil-ion detector with gaussian functions [Fig. 2(b)]. The data were then corrected for the relative detection efficiency obtained for each charge state. For charged recoil ions, the experimental charge-state branching ratios including these corrections are given in Table I. Electron capture probabilities from He buffer gas between the Paul trap and the spectrometer also have

TABLE I. Experimental ion charge-state relative branching ratios (%) and included corrections (see text) compared to calculations with and without recoil and Auger ionizations.

Charge	$\text{MCP}_{\text{corr.}}$	$\text{Tail}_{\text{corr.}}$	Expt. results	With recoil, with Auger	Without recoil, with Auger	With recoil, without Auger	Without recoil, without Auger
1	0.37	−0.17	74.75 ± 1.07	74.37	74.44	87.07	87.37
2	−0.24	−0.09	17.24 ± 0.44	16.98	16.91	11.92	11.66
3	−0.09	0.03	5.71 ± 0.27	6.03	6.04	0.95	0.91
4	−0.03	0.13	1.58 ± 0.21	1.79	1.79	0.05	0.05
>4	−0.01	0.10	0.71 ± 0.18	0.82	0.82	<0.002	<0.002

been estimated using experimental cross sections measured for $Kr^{q+} + He$ collisions in the same velocity regime [22]. Because Kr and Cl have similar ionization potentials, the charge exchange cross sections for Kr^{q+} ions constitute a good approximation of what one would expect with Cl^{q+} ions. Even for the higher charge states involved here ($q = 5$ and 6), these probabilities are only of the order of a few 10^{-4}. They were therefore neglected at the present level of precision. For a dominant part of the decay events, there is no electron shakeoff and the β^+ decay of a $^{35}Ar^+$ ion results in the recoil of a neutral ^{35}Cl atom. For Cl recoil atoms, both the collection efficiency and the MCPPSD detection efficiency are very low, and depend strongly on their initial energy. Because the TOF associated with such detected events is larger than 11 μs, they do not appear on the spectrum shown in Fig. 2(a). To estimate the number of ^{35}Cl atoms produced during the experiment, we have used the number of β particles detected in "singles" (without a condition on the detection of a recoil). Knowing the overall absolute detection efficiency for ions, the fraction of the "singles" events associated with charged ^{35}Cl recoils could be inferred, with the rest being associated to ^{35}Cl atoms. This estimate leads to 72(10)% of neutral ^{35}Cl recoils, with an uncertainty dominated here by the error on the overall ion detection efficiency. This result is in good agreement with the 73.9% ratio obtained from the theoretical calculations that we detail hereinafter.

Subsequent to the sudden decay of $^{35}Ar^+$, primary Cl^{q+} ions are formed by ionization. In the framework of the independent electron model (IPM [23]), which is well suited to describe the dynamics of multielectronic systems, the probability to ionize $q_S = q$ electrons among the $N = 17$ total ones reads

$$P_{q_S}^{\text{ion}} = \sum_{i_1=1}^{N} p_{i_1} \sum_{i_2>i_1}^{N} p_{i_2} \cdots \sum_{i_{q_S}>i_{q_S-1}}^{N} p_{i_{q_S}} \prod_{j\neq i_1,\ldots,i_{q_S}}^{N} (1-p_j), \quad (1)$$

where p_i is the one-electron ionization probability for the ith electron. In our work, p_i results from SO, with the following underlying assumptions: (i) The so-called direct ionization mechanism, in which the β particle knocks out orbital electrons, is neglected, and (ii) shakeup processes, which would imply electron excitation(s) as a result of the β decay, are also neglected. Assumption (i) is consistent with the fact that the β emission energy (with end point $E_\beta^{\max} = 4.94$ MeV) is considerably larger than the energy of bound electrons, so that direct ionization is unlikely [24]. Most of the inelastic processes involving electron vacancies in intermediate- and large-Z species consist of transitions to the continuum [25], justifying (ii). Therefore, the one-electron ionization probability p_i, with i initially belonging to the (n_i, l_i) subshell, is expressed as

$$p_i = 1 - \sum_{n'\leqslant 3} \left|\left\langle \varphi_{n'l}^{(\text{Cl})} \middle| e^{-i\mathbf{K}\cdot\mathbf{r}} \middle| \varphi_{n_i l_i}^{(\text{Ar}^+)} \right\rangle\right|^2, \quad (2)$$

in the rest frame of the daughter nucleus of mass M which recoils with energy E_R and momentum $K = \sqrt{2E_R/M}$ (in atomic units). $\varphi_{nl}^{(\text{Ar}^+,\text{Cl})}$ is the wave function describing one electron orbiting in the nl subshell of Ar^+ or Cl. Because of the small values of K ($E_R^{\max} = 452$ eV), $e^{-i\mathbf{K}\cdot\mathbf{r}}$ can be expanded in Eq. (2) in order to highlight the mechanisms underlying β-induced SO. Up to second order in K^2, we obtain [26]

$$p_i = 1 - \sum_{n'\leqslant 3} \left\{ \left|\left\langle \varphi_{n'l_i}^{(\text{Cl})} \middle| \varphi_{n_i l_i}^{(\text{Ar}^+)} \right\rangle\right|^2 + K^2 \left|\left\langle \varphi_{n'l_i\pm 1}^{(\text{Cl})} \middle| \mathbf{r} \middle| \varphi_{n_i l_i}^{(\text{Ar}^+)} \right\rangle\right|^2 - K^2 \,\text{Re}\left\langle \varphi_{n'l_i}^{(\text{Cl})} \middle| \varphi_{n_i l_i}^{(\text{Ar}^+)} \right\rangle^* \left\langle \varphi_{n'l_i}^{(\text{Cl})} \middle| r^2 \middle| \varphi_{n_i l_i}^{(\text{Ar}^+)} \right\rangle \right\}. \quad (3)$$

It is thus clear that ionization stems from the coherent superposition of two effects: the static Ar^+/Cl orbital mismatch, through the $|\langle \varphi_{n'l_i}^{(\text{Cl})} | \varphi_{n_i l_i}^{(\text{Ar}^+)} \rangle|^2$ terms, and the recoil of the Cl daughter nucleus, through the K^2-dependent terms in Eq. (3).

For the calculation of the recoil-induced ionization terms involved in Eq. (3), we have used the mean recoil energy obtained in our experiment, $\bar{E}_R = 376$ eV, to define the numerical value of K (0.020 74 a.u.). As Ar^+ and Cl are open-shell valence systems, the wave functions $\varphi_{nl}^{(\text{Ar}^+,\text{Cl})}$ have been computed by means of restricted open-shell Hartree-Fock (ROHF) calculations using the GAMESS-US quantum-chemistry package [27]. These wave functions can alternatively be obtained in terms of unrestricted Hartree-Fock (UHF) computations [28], and we found that the ROHF and UHF p_i probabilities differ by less than 1% for all the $1s, \ldots, 3p$ levels [29].

Once inner-shell vacancies have been created in Cl through ionization, radiative and Auger transitions involving higher-lying electrons tend to fill these vacancies. The probabilities associated with these transitions have to be properly introduced in our calculations, especially as Auger processes are known to contribute significantly to the production of high charge states [17]. Kaastra and Mewe [31] have computed the probabilities $\tilde{p}_i^{s,m_i}$ corresponding to the ejection of m_i electrons through Auger cascades after the electron i, element of the inner $n_i l_i$ subshell, has been removed from Cl^{s+}. s is the ionization stage of Cl and corresponds to the number of electrons previously pulled out from the outermost subshells. Consistently with the treatment of multiple SO ionization, the description of multiple vacancies, and related Auger cascades, is performed in the IPM framework. The probability for the ejection of q_S electrons by SO followed by Auger removal of q_A electrons thus reads

$$P_{q_S,q_A} = \sum_{\substack{m_{i_1},\ldots,m_{i_{q_S}} \\ m_{i_1}+\cdots+m_{i_{q_S}}=q_A}} \sum_{i_1=1}^{N} p_{i_1} \tilde{p}_{i_1}^{s,m_{i_1}} \sum_{i_2>i_1}^{N} p_{i_2} \tilde{p}_{i_2}^{s,m_{i_2}} \cdots \sum_{i_{q_S}>i_{q_S-1}}^{N} p_{i_{q_S}} \tilde{p}_{i_{q_S}}^{s,m_{i_{q_S}}} \prod_{j\neq i_1,\ldots,i_{q_S}}^{N} (1-p_j), \quad (4)$$

where $q_S + q_A = q$, the charge state finally observed.

The computed charge-state branching ratios, which consist of the relative populations of Cl^{q+} species among the total ion yield, are compared to their experimental counterparts in Table I. Equation (4) provides a very good agreement with the measurements.

The calculations can then be used to discriminate between the roles of SO and Auger transitions in the production of Cl^{q+} ions. Neglecting Auger decays, i.e., computing the charge-state distribution according to Eq. (1), severely distorts the Cl^{q+} populations: The $q = +1$ population is overestimated by $\sim$13% while multiple SO is inefficient to explain the abundance of $q \geqslant 3$ states. Such an importance of Auger

TABLE II. Main ionization routes leading to Cl^{q+} formation (in %). nl^{-1} refers to primary SO hole creation in the nl subshell of Cl while $m \times e_A$ means emission of m Auger electrons. The asterisk indicates multiple Auger emission.

Cl^+	Cl^{2+}	Cl^{3+}	Cl^{4+}	Cl^{5+}
$3p^{-1}$: **79.83**	$2p^{-1} + 1e_A$: **49.71**	$2s^{-1} + 2e_A^*$: **52.21**	$2s^{-1}3p^{-1} + 2e_A^*$: **36.95**	$1s^{-1} + 4e_A^*$: **35.56**
$3s^{-1}$: **20.16**	$3p^{-2}$: **29.32**	$2p^{-1}3p^{-1} + 1e_A$: **29.36**	$1s^{-1} + 3e_A^*$: **31.02**	$1s^{-1}3p^{-1} + 3e_A^*$: **19.69**
	$3s^{-1}3p^{-1}$: **18.51**	$2p^{-1}3s^{-1} + 1e_A$: **7.41**	$2s^{-1}3s^{-1} + 2e_A^*$: **9.31**	$2s^{-1}2p^{-1} + 3e_A^*$: **15.64**
	$3s^{-2}$: **1.17**	$3s^{-1}3p^{-2}$: **4.37**	$2p^{-1}3p^{-2} + 1e_A$: **8.28**	$2s^{-1}3p^{-2} + 2e_A^*$: **9.26**
		$3p^{-3}$: **3.46**	$2p^{-2} + 2e_A$: **5.86**	$2s^{-1}3s^{-1}3p^{-1} + 2e_A^*$: **5.84**
		$1s^{-1} + 2e_A^*$: **1.56**	$2p^{-1}3s^{-1}3p^{-1} + 1e_A$: **5.23**	$1s^{-1}3s^{-1} + 3e_A^*$: **4.90**
				$2p^{-2}3p^{-1} + 2e_A^*$: **3.66**
				$2p^{-1}3s^{-1}3p^{-2} + 1e_A$: **1.31**

processes has to be contrasted with previous studies on lighter systems, where differences between full and SO-restricted calculations did not exceed a few percent (see, e.g., Ref. [17]). The increase of the Auger importance with increasing Z can be simply related to the higher multiplicity of Auger cascades; for instance, we derive from Ref. [31] that $Cl^+(1s^{-1})$ preferentially stabilizes by emitting three electrons while $Na^+(1s^{-1})$ relaxes by ejecting only one electron.

The calculations also can be employed to estimate the role of recoil-induced ionization by artificially setting $K = 0$ in Eq. (3). The static orbital mismatch explains most of SO ionization (see Table I). However, accounting for the recoil changes the final population of neutral Cl from 74.5% to 73.9%. Even if it looks small at first sight, such a variation can significantly influence the precise determination of the $a_{\beta\nu}$ correlation coefficient [17]. The nuclear recoil is almost inconsequential to the charge-state distribution (Table I). Multiple ionization from primary SO is small (∼3%) so that the relative populations of Cl^{q+} high charge states are mainly monitored by the subsequent Auger cascades.

Finally, we can search within Eq. (4) the electronic probabilities which mostly contribute to the formation of a given Cl^{q+} state. The ionization routes contributing more than 1% to the formation of Cl^{q+}, with $1 \leqslant q \leqslant 5$, are presented in Table II. Single SO from $n = 3$ states explains ∼100% of Cl^+ formation since ionization in inner shells leads to the formation of higher charge states through Auger cascades with almost 100% probability. For Cl^{2+}, twofold SO from the outer $n = 3$ shell, eventually followed by radiative stabilization when $3s$ holes are involved, represents ∼50% of the population and single Auger transitions filling the $2p^{-1}$ SO hole make up the rest. The relevance of SO ionization with a multiplicity greater than 2 rapidly decreases (see Table I). As a result, the creation of Cl^{q+} ions with $q \geqslant 3$ mostly involves Auger decays subsequent to onefold and twofold SO ionization. Moreover, multiple Auger emission, involving intermediate core-hole states and the emission of several electrons during a single-hole decay, becomes increasingly important for high q; it participates to almost 100% of Cl^{5+} ion creation.

To sum up, our joined experimental and theoretical endeavor has provided a quite complete picture of ion formation resulting from the β^+ decay of $^{35}Ar^+$. We plan to apply the same techniques to $^{19}Ne^+$ and also revisit previous studies [17] in the near future. Besides the intrinsic interest in such investigations to nuclear physics, this will allow for one to obtain a more complete and Z-dependent picture of the underlying ionization mechanisms.

The authors thank the LPC staff for their strong involvement in the LPCTrap project and the GANIL staff for the preparation of a high-quality ion beam. The authors also acknowledge the computational facilities provided by the Mésocentre de Calcul Intensif Aquitain at the University of Bordeaux [32]. D.R. acknowledges support from the Spanish Ministry of Economy and Competitiveness under Project No. FPA2010-14803 and Action No. AIC10-D-000562.

[1] D. R. Hamilton, Phys. Rev. **71**, 456 (1947).
[2] J. S. Allen, R. L. Burman, W. B. Herrmannsfeldt, P. Stähelin, and T. H. Braid, Phys. Rev. **116**, 134 (1959).
[3] C. H. Johnson, Frances Pleasonton, and T. A. Carlson, Phys. Rev. **132**, 1149 (1963).
[4] N. Severijns and O. Naviliat-Cuncic, Annu. Rev. Nucl. Part. Sci. **61**, 23 (2011).
[5] A. Gorelov *et al.*, Phys. Rev. Lett. **94**, 142501 (2005).
[6] P. A. Vetter, J. R. Abo-Shaeer, S. J. Freedman, and R. Maruyama, Phys. Rev. C **77**, 035502 (2008).
[7] X. Fléchard, Ph. Velten, E. Liénard, A. Méry, D. Rodríguez, G. Ban, D. Durand, F. Mauger, O. Naviliat-Cuncic, and J. C. Thomas, J. Phys. G **38**, 055101 (2011).
[8] D. Rodríguez *et al.*, Nucl. Instrum. Methods Phys. Res. A **565**, 876 (2006).
[9] X. Fléchard *et al.*, Phys. Rev. Lett. **101**, 212504 (2008).
[10] C. Couratin *et al.*, Phys. Rev. Lett. **108**, 243201 (2012).
[11] T. A. Carlson, W. E. Hunt, and M. O. Krause, Phys. Rev. **151**, 41 (1966).
[12] N. Saito and I. H. Suzuki, Phys. Scr. **49**, 80 (1994).
[13] P. Persson, S. Lunell, A. Szöke, B. Ziaja, and J. Hajdu, Protein Sci. **10**, 2480 (2001).
[14] T. Kaneyasu, Y. Hikosaka, E. Shigemasa, P. Lablanquie, F. Penent, and K. Ito, J. Phys. B **41**, 135101 (2008).
[15] T. A. Carlson, Phys. Rev. **131**, 676 (1963) and references therein.

[16] A. Gorelov *et al*., Hyperfine Interact. **127**, 373 (2000).
[17] N. D. Scielzo, S. J. Freedman, B. K. Fujikawa, and P. A. Vetter, Phys. Rev. A **68**, 022716 (2003).
[18] M. Beck *et al*., Eur. Phys. J. A **47**, 45 (2011).
[19] S. Van Gorp *et al*. (unpublished).
[20] G. Darius *et al*., Rev. Sci. Instrum. **75**, 4804 (2004).
[21] E. Liénard *et al*., Nucl. Instrum. Methods Phys. Res. A **551**, 375 (2005).
[22] E. Justiniano, C. L. Cocke, T. J. Gray, R. Dubois, C. Can, W. Waggoner, R. Schuch, H. Schmidt-Böcking, and H. Ingwersen, Phys. Rev. A **29**, 1088 (1984).
[23] B. H. Bransden and M. H. C. McDowell, *Charge Exchange and the Theory of Ion-Atom Collisions* (Clarendon, Oxford, UK, 1992).
[24] M. S. Freedman, Annu. Rev. Nucl. Sci. **24**, 209 (1974).
[25] T. A. Carlson, Phys. Rev. **130**, 2361 (1963).
[26] T. A. Carlson, F. Pleasonton, and C. H. Johnson, Phys. Rev. **129**, 2220 (1963).
[27] M. W. Schmidt *et al*., J. Comput. Chem. **14**, 1347 (1993).
[28] J. A. Pople and R. K. Nesbet, J. Chem. Phys. **22**, 571 (1954).
[29] It is quite common to employ the Roothan-Hartree-Fock (RHF) orbitals of Clementi and Roetti [30] to compute the ionization probabilities p_i. Even though we employ a different (and larger) underlying basis to construct the Ar^+ and Cl orbitals, we have verified that the p_i values obtained with the orbitals of Clementi and Roetti differ by less than 1% from our ROHF and UHF values.
[30] E. Clementi and C. Roetti, At. Data Nucl. Data Tables **14**, 177 (1974).
[31] J. S. Kaastra and R. Mewe, Astron. Astrophys. Suppl. Ser. **97**, 443 (1993).
[32] http://www.mcia.univ-bordeaux.fr